AD-A166 456 NUMERICAL SIMULATION OF A LOW DENSITY PLASMA EROSION OPENING SWITCH(U) NAVAL RESEARCH LAB WASHINTTON DC J M GROSSMANN ET AL. 19 MAR 86 NRL-MR-5724 1/1

UNCLASSIFIED F/G 20/9 NL

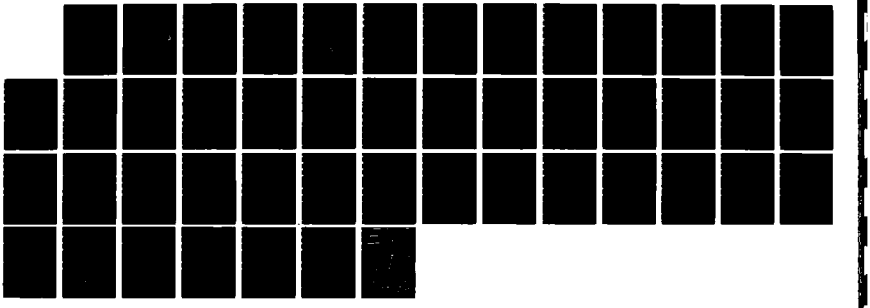

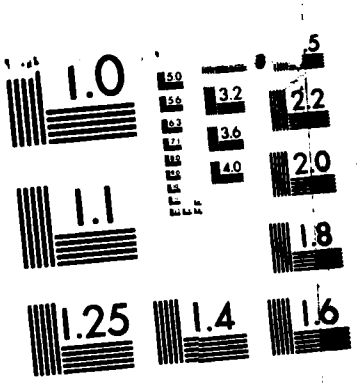

MICROCOPY RESOLUTION TEST CHART
NATIONAL BUREAU OF STANDARDS-1963-A

AD-A166 456

NRL Memorandum Report 5724

Numerical Simulation of a Low Density Plasma Erosion Opening Switch

J. M. GROSSMANN, P. F. OTTINGER, J. M. NERI AND A. T. DROBOT*

Plasma Technology Branch
Plasma Physics Division

**Science Applications International Corporation*
McLean, VA 22102

DTIC
ELECTE
APR 9 1986
S D
B

March 19, 1986

This work was supported in part by the U.S. Department of Energy and the Office of Naval Research.

NAVAL RESEARCH LABORATORY
Washington, D.C.

DTIC FILE COPY

Approved for public release; distribution unlimited.

AD-A166456

SECURITY CLASSIFICATION OF THIS PAGE

REPORT DOCUMENTATION PAGE

1a. REPORT SECURITY CLASSIFICATION UNCLASSIFIED	1b. RESTRICTIVE MARKINGS
2a. SECURITY CLASSIFICATION AUTHORITY	3. DISTRIBUTION/AVAILABILITY OF REPORT Approved for public release; distribution unlimited.
2b. DECLASSIFICATION/DOWNGRADING SCHEDULE	
4. PERFORMING ORGANIZATION REPORT NUMBER(S) NRL Memorandum Report 5724	5. MONITORING ORGANIZATION REPORT NUMBER(S)
6a. NAME OF PERFORMING ORGANIZATION Naval Research Laboratory 6b. OFFICE SYMBOL (If applicable) Code 4771	7a. NAME OF MONITORING ORGANIZATION
6c. ADDRESS (City, State, and ZIP Code) Washington, DC 20375-5000	7b. ADDRESS (City, State, and ZIP Code)
8a. NAME OF FUNDING/SPONSORING ORGANIZATION DOE and ONR 8b. OFFICE SYMBOL (If applicable)	9. PROCUREMENT INSTRUMENT IDENTIFICATION NUMBER
8c. ADDRESS (City, State, and ZIP Code) Washington, DC 20547 Arlington, VA 22217	10. SOURCE OF FUNDING NUMBERS PROGRAM ELEMENT NO. (See page ii) / PROJECT NO. / TASK NO. / WORK UNIT ACCESSION NO.

11. TITLE (Include Security Classification)
Numerical Simulation of a Low Density Plasma Erosion Opening Switch

12. PERSONAL AUTHOR(S)
Grossmann, J. M., Ottinger, P. F., Neri, J. M. and Drobot, A. T.*

13a. TYPE OF REPORT	13b. TIME COVERED	14. DATE OF REPORT (Year, Month, Day)	15. PAGE COUNT
Interim	FROM ____ TO ____	1986 March 19	47

16. SUPPLEMENTARY NOTATION *Science Applications International Corporation, McLean, VA 22102
This work was supported in part by the U.S. Department of Energy and the Office of Naval Research.

17. COSATI CODES		
FIELD	GROUP	SUB-GROUP

18. SUBJECT TERMS (Continue on reverse if necessary and identify by block number)
Fast opening switches
Numerical simulation of plasmas
Current conduction in plasmas
Pulse compression
Pulsed power

19. ABSTRACT (Continue on reverse if necessary and identify by block number)
The conduction of current through a low density ($\sim 10^{12}$ cm^{-3}) collisionless plasma injected between two coaxial conducting cylinders is simulated using a 2 1/2D, electromagnetic particle-in-cell code. Plasma is injected through the anode towards the cathode with flow velocity, V_F, and is assumed to be azimuthally symmetric. Current is driven through the plasma so that the 100 kA level is reached in $\sim$5 ns. The opening process, when current is diverted to a load, is also treated. Electrons are found to carry current in a narrow current channel across the plasma by $E \times B$ drift. A large electric field is established by charge separation in the plasma in order to provide the drift. The motion of the anode end of the current channel controls the time of opening and is found to be independent of V_F and to depend strongly on density and length.

20. DISTRIBUTION/AVAILABILITY OF ABSTRACT	21. ABSTRACT SECURITY CLASSIFICATION
☒ UNCLASSIFIED/UNLIMITED ☐ SAME AS RPT. ☐ DTIC USERS	UNCLASSIFIED
22a. NAME OF RESPONSIBLE INDIVIDUAL J. M. Grossmann	22b. TELEPHONE (Include Area Code) (202) 767-3066 22c. OFFICE SYMBOL Code 4771

DD FORM 1473, 84 MAR 83 APR edition may be used until exhausted. All other editions are obsolete.

SECURITY CLASSIFICATION OF THIS PAGE

10. SOURCE OF FUNDING NUMBERS

PROGRAM ELEMENT NO.	PROJECT NO.	TASK NO.	WORK UNIT ACCESSION NO.
DOE 61153N		23 RR011-09-41	DN680-382 DN320-105

CONTENTS

I. INTRODUCTION 1

II. NUMERICAL SIMULATIONS 5

III. RESULTS 9

IV. DISCUSSION 14

V. CONCLUSIONS 27

ACKNOWLEDGMENTS 29

REFERENCES 42

DTIC ELECTE APR 9 1986 S D B

Accession For
NTIS GRA&I ☑
DTIC TAB ☐
Unannounced ☐
Justification
By
Distribution /
Availability Codes
Dist | Avail and/or Special
A-1

QUALITY INSPECTED 3

NUMERICAL SIMULATION OF A LOW DENSITY PLASMA EROSION OPENING SWITCH

I. Introduction

The presence of plasma in the vacuum output transmission line of a pulsed power generator can enhance or degrade the power pulse delivered to the vacuum load. The uncontrolled generation of high density plasma in the vacuum line generally degrades the coupling of the generator to the load by providing an alternative path for the generator current. In the worst case, the entire generator current can be shunted away from the load by the plasma. Sources of uncontrolled plasma include intense UV irradiation of surfaces and plasmas from explosive field emission. However, by injection of low density plasmas into the vacuum line, the alternative current path to ground through the plasma can be controlled as a function of time, and the power pulse delivered to the load intentionally modified.

In particular, the geometry of the vacuum transmission line and the properties of the injected plasma can be chosen so that a plasma erosion opening switch (PEOS) configuration[1] is obtained, as illustrated in Fig. 1. Originally this configuration was successfully used as a plasma erosion switch (PES) for prepulse suppression,[2] which suggested its potential as an opening switch.[3] As an opening switch the PEOS can be used for inductive storage applications. The switch plasma conducts the generator current for some period of time, while the energy of the generator is stored inductively in the vacuum transmission line between the generator and the plasma. At a predetermined time, the plasma will cease to act as a low impedance path to ground, and the current will be swiftly diverted to the load. This inductive

Manuscript approved November 4, 1985.

storage/PEOS technique modifies the output of the generator to deliver a similar current, higher voltage, shorter duration pulse to the load. The generator can charge the vacuum inductor at a voltage less than the load voltage, reducing voltage stress on the generator vacuum insulator and limiting the uncontrolled production of plasma in the vacuum transmission line. High voltage at the load exists only after the PEOS opens at a time when most of the generator energy is already stored in the vacuum section. Significant power and voltage multiplication (compared with the case of no PEOS) is obtained only if the opening time of the PEOS is much shorter than the conduction phase of the PEOS. The proper plasma conditions[4] are crucial for achieving the required fast opening time.

The work presented in this paper treats the conduction of current through a low density ($\sim 10^{12} cm^{-3}$) collisionless plasma injected between two coaxial conducting cylinders as illustrated in Fig. 1. The plasma is injected through the anode towards the cathode with a flow velocity, V_F, and is assumed azimuthally symmetric. The opening process, when current is diverted to a load, is also treated. The 2 1/2 D electromagnetic particle-in-cell code, MASK,[5] is used to simulate the problem. Current is driven through the plasma so that the 100 kA level is reached in $\sim$ 5 ns. Space charge limited electron emission is allowed on the conducting surfaces and particles encountering the surfaces are absorbed. A partially transmitting boundary condition at the load end is used to simulate a terminating load impedance.

Results show that initially a narrow radial current channel forms at the generator side of the plasma. The current carrying electrons include both plasma electrons and electrons emitted from the cathode. The electrons are bent slightly toward the load by the $\underline{v}_r \times \underline{B}_\theta$ force as they travel toward the anode where they are absorbed. Generally their early trajectories are predominately radial, but the slight bending of their orbits produces an axial

displacement of electrons (and space charge buildup) toward the load. This results in a layer of negative space charge on the load side of the current channel and a layer of positive space charge on the generator side of the current channel and thus a strong axial electric field in the current channel. As the current increases, electrons can then $\underline{E} \times \underline{B}$ drift radially across the magnetic field lines. The axial electric field is shorted out at the anode and cathode.

At the cathode the induced radial electric field is enhanced by the electric field associated with the space charge region in the current channel. This large radial field produces the necessary electron emission from the cathode and radially accelerates these electrons into the current channel. At the anode the induced radial electric field is reduced by the electric field associated with the space charge region in the current channel. The anode end of the current channel propagates downstream toward the load, while the cathode end of the channel where electrons enter the channel (emission site), moves only slightly (depending only on the $\underline{J} \times \underline{B}$ force). Thus the channel orientation begins by being radial, but becomes more and more diagonal as the current increases.

The migration of the anode end of the current channel is caused by electrons $\underline{E}_r \times \underline{B}_\theta$ drifting axially toward the load and neutralizing the ion space charge. These electrons enter the system from the anode and fill in behind the current channel on the generator side as it moves toward the load. When the current channel reaches the load end of the plasma, the axial space charge electric field can no longer be maintained. At this time the electron flow is quickly magnetically insulated and the current is diverted to the load. While the plasma conducts current, the current channel remains narrow (i.e., much less than the plasma width) and the current density

increases. The plasma flow velocity has little effect on the time of opening or current density. The width of the channel is determined by the amount of space charge buildup required to produce the proper electric field and the associated $\underline{E}x\underline{B}$ drift velocity for current conduction. In the case of low mass density (e.g., when the ion species is protons), significant $\underline{J}x\underline{B}$ axial displacement of the emission site and current channel also occurs.

As set up, this problem is designed to be the first step in simulating a low density ($\sim 10^{12}cm^{-3}$), high flow velocity ($\sim 10^{8}cm/sec$) PEOS. Scaling from present experimental results[6] to high voltage applications[7] of the PEOS, such as for PBFA II, leads to consideration of PEOS operation in this low density, high flow velocity regime. However, because the simulations treat this new regime, the physical processes controlling the PEOS operation may not be the same as observed in the higher density experiments. In fact, the results presented here and in previously reported work,[8] are not consistent with either the experimental results[6] at higher density ($\sim 10^{13}cm^{-3}$) or the theoretical model[4] which has been used to explain these higher density PEOS experiments. For example, experimental results[9,6] show that the current channel broadens as the current increases while the current density remains approximately constant. The switch opens when the current channel width reaches the full width of the plasma. The current density in the plasma is proportional to the ion flux density, $n_i V_F$, at the cathode. These results are not reproduced in the simulations. There are, however, fundamental differences in the two problems. In the simulations: a) the density is an order of magnitude lower; b) the dI/dt is a factor of five larger (which is more similar to the current risetime of PBFA II); c) the timescale is an order of magnitude shorter; d) the plasma electron temperature is more than two orders of magnitude higher and e) azimuthal symmetry is imposed. The presence

of anomalous collisions due to instabilities could reconcile the experimental and simulation results by allowing electrons to cross magnetic field lines and carry current radially across the switch. This would eliminate the need for the large space charge separation and electric fields found to be required in these simulations for $\underline{E} \times \underline{B}$ current flow. In addition the emission would spread further across the cathode than in the present simulations because the local enhancement of emission due to the large space charge separation would not be present. This collisional current carrying mechanism could give results more similar to those observed experimentally; however, it is precluded from appearing in the present simulations because of the differences a) through e) discussed above. This mechanism will be studied in future work.

In Sec. II the numerical simulations are discussed in detail, including all assumptions and boundary conditions. In Sec. III the results of the simulations are presented. Results are shown for different ion species, different densities, different plasma injection velocities and different current risetimes. A detailed discussion of the results is given in Sec. IV and Sec. V includes a discussion of the conclusions that can be drawn from this work. Plans for extending this work to include the effects of anomalous collisions are also discussed in the last section.

II. Numerical Simulations

The problem to be simulated deals with the conduction of current through a low density ($\sim 10^{12} cm^{-3}$) collisionless plasma injected between two coaxial conducting cylinders as shown in Fig. 1. The opening process, during which current is diverted to the load, is also dealt with. This is the first step in simulating the low density operation of a PEOS. The 2 1/2-D electromagnetic particle-in-cell code MASK is used to properly treat both the

switch plasma and the boundary emission of electrons into the plasma. The problem is done in r-z geometry and azimuthal symmetry is imposed. Simulations were also run in planar geometry. Aside from geometry effects, the current conduction and opening process were similar; therefore only the cylindrical geometry cases will be discussed here.

The coaxial electrodes and the switch plasma form part of a circuit with a generator at the left and a load in parallel with the switch at the right. The generator in the simulations is modeled as a current source with current rising linearly from 0 to 100 kA in about 5 ns. The anode and cathode are perfect conductors, while the boundary at the load is given an "impedance" by specifying a transmission coefficient for electromagnetic waves incident on the radial surface. The cathode radius is 2.5 cm, and the anode radius is 5 cm. The simulation region is 12.8 cm long axially, with the plasma occupying the volume between z = 2.5 cm and z = 7.5 cm. The regions on both sides of the plasma between the plasma and the axial boundaries are vacuum regions. The cathode and anode boundaries are also the sources of ions and electrons. Plasma electrons and ions are injected down from the anode between z = 2.5 cm and 7.5 cm with flow velocity $V_F = 1.8 \times 10^8$ cm/s. Electrons are also allowed to be emitted from both the cathode and anode as required by space charge limited emission. Particles striking any of the boundaries are absorbed. The initial plasma fill itself is also given a flow velocity toward the cathode of $V_F = 1.8 \times 10^8$ cm/s and has a density of $n_o = n_i = n_e = 10^{12}$ cm^{-3}. A cold start is used whereby cold electrons and ions are initially placed directly on top of each other and given a radially inward flow velocity.

The simulation region is divided into a 128 (in z) by 50 (in r) mesh, which is uniform in each direction. The mesh sizes are then $\Delta r = 0.05$ cm and $\Delta z = 0.1$ cm. Four macroparticles of each specie are used initially in each cell in the plasma region. Simulations run with different numbers of

macroparticles per cell showed that this was about the minimum number needed to maintain good particle statistics. Larger numbers of macroparticles per cell produced similar results. The skin depth for the plasma with n_o = $10^{12}cm^{-3}$ is about c/ω_{pe} = 0.5 cm, and is easily resolved in all the simulations to ensure accurate attenuation of the fields by the plasma. In addition, the simulation region is broad enough to prevent the fields from leaking through to the load before opening.

Some numerical questions of concern include the resolution of the Debye length and the correct treatment of the electron emission region. The experimentally measured value for the initial plasma temperature in a PEOS configuration is about T_p = 5 eV.[6] This would require a prohibitively small mesh size to resolve the Debye length. Since it is important to simulate the full switch region in order to investigate both current conduction and switch opening, an artificially high plasma temperature is used. This temperature is specified by equating the mesh size with the Debye length for a given plasma density. Using a cold start this temperature is quickly reached (< 1 ns) by numerical heating, which ends after the Debye length increases to the mesh size. Simulations performed with an initially warm plasma, T_e = $4\pi n_e e^2(\Delta r)^2$, show identical mechanisms of current conduction and switch opening. This test verifies that the cold start can be used since the early numerical heating does not influence the general switch behavior.

The artificially high plasma temperature and corresponding large mesh size, however, can have an important effect on the simulation results. The large mesh size eliminates smaller wavelength instabilities and waves, and the high temperature can reduce the growth rate and even stabilize those streaming instabilities with wavelengths that can be resolved. The imposition of azimuthal symmetry could also suppress certain instabilities because only m = 0 modes are allowed. These initial simulations are not intended to

address the effect of plasma instabilities on switch behavior; however, a comparison of the simulation results with experimental data demonstrates the importance of further investigations of the role of plasma instabilities and anomolous resistivity. This will be left for future work.

The large mesh size used in the simulations also sets a limit on the size of the space charge limited emission gap, d, that can be resolved at the conducting boundaries. For a given gap voltage, ϕ_g, this in turn limits the available emitted current density to $J = \alpha \phi_g^{3/2}/d^2$. The mesh size in the gap normal direction is chosen in the simulations to resolve the Debye length associated with the energy of emitted electrons. Thus the emission of electrons is not affected by numerical effects. A simulation with a smaller radial mesh size was run to test the numerical treatment of the emission sites. Results verify that the emission processes are being treated accurately.

In the next section, the results of the simulations will be discussed. Simulations have been run at densities of $n_o = 5\text{x}10^{11}\text{cm}^{-3}$ and at $1\text{x}10^{12}\text{cm}^{-3}$. The current risetime, t_r, has also been varied with current reaching 100 kA in 5 ns and 10 ns. Results using both H^+ and C^+ ions are discussed as well as results using different plasma flow velocities. Parameters for the runs that will be discussed are given in Table I. An analysis of switch behavior for each run will be given and compared with the other runs.

Table I: Parameters for each of five simulation runs.

Run #	n (cm^{-3})	t_r (ns)	Species	V_F (cm/μs)
1	$1\text{x}10^{12}$	5	H^+	180
2	$0.5\text{x}10^{12}$	5	H^+	180
3	$1\text{x}10^{12}$	10	H^+	180
4	$1\text{x}10^{12}$	5	C^+	180
5	$1\text{x}10^{12}$	5	H^+	0

III. Results

This section will be devoted to the presentation of results obtained from the computer simulations. Simulations of the five different cases shown in Table I are discussed here, but the physical interpretation of the results is left for the next section. The different simulations have many aspects in common. Switch operation is qualitatively the same for all five cases, with differences appearing in such things as the timing of switch opening and the speed of current channel motion downstream. Four identifiable aspects of switch operation are: 1) early current channel formation, 2) movement of the anode end of the channel toward the load, 3) movement of the cathode end of the channel toward the load, and 4) switch opening by magnetic insulation of the electrons. These four processes can be seen in the series of Figs. 2-4. These plots are snapshots taken of various computational diagnostics at times $t = 0.4$, 3.0, 4.0, 5.0 and 6.0 ns from Case 1 in Table I, which will be used as the model problem here. Plots between 0.4 and 3.0 ns have been omitted because very little activity occurs there and because the numerical heating mentioned in Section II obscures the results between 0.6 and 1.2 ns.

In Fig. 2 current density vectors are plotted in the computational region. At $t = 0.4$ ns (Fig. 2a) current flows between the anode and cathode at the generator side of the plasma. The current remains confined in a channel that never broadens more than about 1 cm as it penetrates through the plasma. The channel evolves in time as seen in Figs. 2b-2e. The anode end of the current channel propagates towards the load through the plasma region faster than the cathode end. Eventually, as shown in Fig. 2e current no longer crosses between anode and cathode in the region of the plasma but has been diverted to the load. Switch opening is defined as the point when 90% or more of the generator current has been switched to the load. For Case 1 in

Table I, the switch conducts current for about 5 ns before reaching this opening point.

The evolution of the electrons and ions in the switch is shown in Figs. 3 and 4. The electrons in Fig. 3 include the original plasma electrons, the emitted electrons and the electrons injected from the anode at the plasma flow velocity. Early in time ($t \lesssim 0.4$ ns), electrons at the generator side of the plasma are accelerated toward the anode, leaving a gap in the lower left corner. This gap remains occupied by the plasma ions, whose space charge elicits electron emission into the gap. The electrons at the generator side of the plasma at $t = 0.4$ ns have been displaced slightly toward the load, thereby exposing a layer of ions along that edge. At all times the current across the switch is carried predominantly by the electrons, so that the electron particle plots can be seen to follow the current channel plots described earlier. Current carrying electrons are emitted from the cathode and either enter the current channel directly (because they have been emitted near the cathode end of the channel) or enter the current channel after flowing downstream along the cathode in a magnetically insulated manner until they reach the current channel. The orbits of these electrons will be shown later in Fig. 5a. Two special features of Fig. 3 should be noted. As the anode end of the channel moves downstream, a diagonal depletion layer is seen in the electron distribution. This depletion layer evolves from the layer of exposed ions seen along edge of the plasma on the generator side at $t = 0.4$ ns. The layer develops as the anode end of the current channel moves toward the load. By $t = 3$ ns, the layer extends diagonally from the original gap region at the cathode on the generator side all the way to the anode nearly at the load end. This depletion layer grows in time, with the current channel forming its boundary on the load side. The ion space charge in the depletion

layer contributes to the electrostatic electric field necessary for the $\underline{E} \times \underline{B}$ drift of the electrons across the switch. Late in time ($t > 5$ ns) the electron motion is almost completely magnetically insulated, with more than 90% of the current flowing along the cathode to the load.

The other notable feature of the electron particle plots is the block of electrons in the upper left hand corner that defines the boundary on the generator side of the depletion layer. These electrons consist largely of electrons emitted and injected from the anode surface which attempt to neutralize the ion space charge in the depletion layer. The orbits of these electrons will be shown later in Fig. 5b. Their role in controlling the motion of the anode end of the current channel will be discussed in Section IV.

The electron behavior should be compared with the ion particle plots seen in Fig. 4. At $t = 0.4$ ns, ions have not had enough time to react and are seen in their original configuration. At later times, a comparison of the electron and ion plots shows that although ions occupying the electron depletion layer have a local density much larger than the local electron density, they have a reduced density compared with the original plasma fill. Also seen in the ion plots is the formation and motion of a high density layer of ions. This structure is formed when ions are accelerated toward the load by the electric field in the current channel that produces the $\underline{E} \times \underline{B}$ drift of the electrons. This is a manifestiation of $\underline{J} \times \underline{B}$ acceleration. This layer of ions acts like a leaky piston, picking up a certain fraction of ions as it moves downstream. The ions left behind by the piston occupy the electron depletion layer mentioned earlier. The position of the piston marks the cathode end of the current channel because the ion space charge in the piston stimulates the emission of current carrying electrons directly into the channel. Other

electrons generally enter the channel after being emitted on the generator side of the current channel and flowing along the cathode until reaching the radial current channel. At t = 5 ns, most of the ions in the piston have been absorbed at the cathode, leaving only a small clump of ions at the lower right corner of the plasma. These ions are responsible for the spray of electrons in the corresponding electron plot. One final feature to note is that ions which are continually injected at the anode fill in behind the depletion layer on the generator side at the original plasma density.

Typical electron trajectories in the current channel are shown in Fig. 5 at t ~ 4 ns. Note that the cathode end of the current channel is at ~ 4.5 cm while the anode end is at ~ 7.25 cm. Figure 5a illustrates that the trajectories of many of the current carrying electrons are straight and that even those electrons which do execute perpendicular gyromotion can cross the A-K gap in very few gyroperiods. The importance of this observation is made clear in Section IV. The electrons in Fig. 5b are executing orbits in the region of plasma on the generator side of the current channel. These electrons attempt to neutralize the space charge in the electron depletion layer. They $\underline{E} \times \underline{B}$ drift axially into the depletion layer, thereby reducing the local ion space charge. Consequently, the electron current channel moves toward the load in order to maintain the space charge separation required for the $\underline{E} \times \underline{B}$ drift current conduction.

The differences in the behavior of the switch for the various cases listed in Table I are predominantly ones of timing. All four aspects of switch behavior discussed earlier are present in all five cases. In Figs. 6 and 7, the relative motion of the anode end of the current channel and the piston motion along the cathode (or the motion of the cathode end of the current channel) are shown for all five cases. Figure 6 demonstrates that the

motion of the anode end of the channel is approximately logarithmic in time. Figure 7 demonstrates a nearly parabolic motion for the ion piston. Analytic interpretations and explanations of these characteristics will be given in the next section.

Finally, a comparison is made in Table II of the approximate times of opening for the different cases in Table I. The time of opening is defined as the point when 90% or more current is diverted to the load. This can be compared with the time when only about 10% of the current is diverted to the load, also shown in Table II. In all respects, other than timings, the current carried by the switch plasmas for the various cases evolves very much like Case 1. In Fig. 8, magnetic "probe" data for Case 1 is exhibited for two probes at $r = 4.6$ cm. One probe ($z = 2.8$ cm) is just inside the upstream boundary of the original plasma configuration, the other lies close to the load ($z = 12$ cm). The probe near the load shows that the switch plasma conducts more than 90% of the current presented to it until about $t = 2$ ns, at which point the switch can be said to begin to open and allow more and more current to flow to the load. At $t = 5$ ns 90% of the current is flowing through the load.

Table II: Time at which 10% and 90% of the total current begins to flow in the load for each of the five runs listed in Table I.

Case	10% point (ns)	90% point (ns)
1	2.0	5.0
2	1.6	3.5
3	3.6	6.5
4	2.8	5.9
5	2.2	5.1

In the next section, the data presented here is interpreted and analyzed to understand the underlying physics of the switch behavior discussed in this section.

IV. Discussion

In Sec. III the results of several runs demonstrated current conduction and opening under different plasma conditions. The features that these simulations display are now discussed and compared. In Sec. III, Case 1 in Table I was used as a baseline for comparison because it best illustrates all the features of the switch behavior. Although Case 1 is still used for comparisons, in this section Case 4 in Table I is used as a baseline for much of the analysis. Because of the higher mass C^+ ions in Case 4, the analysis of the other physical effects can be carried out without being obscured by $\underline{J} \times \underline{B}$ ion motion. Early time current conduction and current channel formation are discussed first. The mechanisms involved in current conduction in this channel are discussed next, together with an examination of the role that electron orbits play in determining the width of the channel. Following this the evolution of the channel in time is described including $\underline{J} \times \underline{B}$ effects. This section concludes with a comparison of the five runs within the context of this discussion.

Very early in time, current is carried at the generator side of the plasma by plasma electrons accelerated radially towards the anode by the induced radial electric field. The plasma prevents the fields from penetrating more than about a skin depth ($c/\omega_{pe} \sim 0.5$ cm) into the switch region. The current carrying electrons are also displaced slightly toward the load by the $\underline{v} \times \underline{B}$ force, resulting in a thin layer ($\lesssim 0.5$ cm) of space charge and a self-consistent axial electric field as illustrated in Fig. 9a. The

massive ions are unable to respond on a fast timescale; however on a longer timescale, ion acceleration in the electric field is a manifestation of the single fluid $\underline{J} \times \underline{B}$ force. On the shorter timescale the axial electric field provides an $\underline{E} \times \underline{B}$ drift channel on the load side of this space charge layer for radial electron current conduction. The ion gyroperiod is long compared with the time scale of interest so that ion $\underline{E} \times \underline{B}$ drift motion is not important. Electron trajectories are basically straight, carrying the electrons radially from the cathode toward the anode in this channel.

Because the axial electric field must vanish at the conducting cathode, another mechanism must be responsible for transporting the electrons from the cathode surface to this drift channel. The initial radial flow of plasma electrons leave behind a region of exposed ions or gap between the plasma and the cathode at the generator side of the plasma as was seen in Fig. 3a. The space charge associated with these ions locally enhances the induced radial electric field and hence the emission of electrons from the cathode. These electrons are accelerated across this gap and enter the $\underline{E} \times \underline{B}$ drift channel to be carried across to the anode. In order to cross the gap the effective electron gyroradius must be large compared with the gap size.

At early times when electrons enter the $\underline{E} \times \underline{B}$ drift channel, they flow in a nearly force-free fashion. That is to say the force from the electric field is nearly balanced by the $\underline{v} \times \underline{B}$ force so that the $\underline{E} \times \underline{B}$ drift velocity of the electrons is much larger than the velocity associated with oscillations about the force-free trajectory (later in time larger oscillations are observed). This force-free flow is stable in a fluid sense, in that perturbations in the current channel position produce forces which restore the channel to its original position. If the electron current channel were displaced toward the load more space charge would be produced and the electric field would be

increased. This unbalanced electric field would pull the channel back toward the generator and its original position. Similarly if the electron current channel were displaced toward the generator the space charge would be reduced as well as the electric field. The unbalanced $\underline{v} \times \underline{B}$ force would now draw the current channel back toward the load and its original position. Thus current conduction provided by the $\underline{E} \times \underline{B}$ radial drift of electron across the plasma is stable.

Consider now the space charge layer and $\underline{E} \times \underline{B}$ drift channel in more detail. These structures are illustrated schematically in Fig. 9a. The width of the space charge layer is controlled by the electric field required to carry the instantaneous current, I(t). The width can be estimated by assuming that an annulus of electrons of density αn is displaced toward the load a distance equal to its width, w. Here $\alpha(t) < 1$. The total width of the current channel and the ion layer is 2w. The resulting electric field then provides the electron drift, $v_D \sim Ec/B$, for current conduction with

$$I = 2\pi rwJ = 2\pi rwn(\alpha+1)eEc/B. \tag{1}$$

Poisson's Equation can be used to estimate E yielding

$$E \approx 4\pi n\alpha ez \equiv E_0 z/w, \qquad 0 < z < w. \tag{2}$$

Here $z = 0$ at the load end of the current channel and increases moving toward the generator. Similarly Ampere's Law can be used to calculate B as

$$B \approx 2Iz/wrc \equiv B_0(r)z/w, \qquad 0 < z < w. \tag{3}$$

The width of the current channel is then

$$w(t) = I(t)/(2\pi rnec[\alpha(\alpha+1)]^{1/2}). \tag{4}$$

The drift velocity can also be expressed as $v_D = c(\alpha/1+\alpha)^{1/2}$. If α approaches unity, then v_D approaches $c/\sqrt{2}$. From the simulation with C^+ (Case 4 in Table I) w quickly grows to $\lesssim$ 0.5 cm in the first nanosecond and then grows slowly while $\alpha(t)$ starts out small and approaches unity as I(t) increases. At 4 ns, I = 80 kA, and $\alpha \sim 0.35$, so that from Eq. (2) $w \sim 1.0$ cm for $n = 10^{12}$ cm^{-3} and r = 3.5 cm. Thus at late times the electrons drift at nearly $c/\sqrt{2}$. This is in reasonable agreement with the simulation results. When $\underline{J} \times \underline{B}$ acceleration causes significant ion motion, n actually increases in the current channel. Increased density in turn reduces the required w and/or α. This is evident in the simulations at late times ($t \sim 5$ ns) for carbon ions in Case 4, and plays an important part even at early times for the proton cases.

Electron motion in the $\underline{E} \times \underline{B}$ drift channel can be analyzed nonrelativistically by assuming static fields and using a slab geometry. The assumption that the fields do not vary in time is reasonable because the electron gyroperiod, $2\pi/\omega_{ce}$, is ~ 0.1 ns and because the electrons in the current channel cross from the cathode to the anode in $\lesssim$ 1 ns, both of which are short compared with the 5-10 ns current risetimes in the simulations. The nonrelativistic treatment and the use of slab geometry are for simplicity. The equations of motion for the electrons are then

$$\frac{dv_x}{dt} = \frac{ev_z B_{oz}}{m_e cw}, \tag{5}$$

$$\frac{dv_z}{dt} = \frac{eE_0 z}{m_e w} - \frac{ev_x B_0 z}{m_e cw} , \tag{6}$$

where E_0 and B_0 are defined as in Eqs. (2) and (3) and the same coordinate system is used as in Eqs. (2) and (3) with x measuring in the direction from the cathode to the anode. By transforming to a frame drifting at the $\underline{E} \times \underline{B}$ drift velocity, $v_D = E_0 c/B_0$, the electron motion is found to involve a constant drift velocity and a gyromotion, $\underline{v}_g = \underline{v} - v_D \hat{\underline{e}}_x$, described by

$$\frac{dv_{gx}}{dt} = \frac{\omega_{co} v_{gz} z}{w} , \tag{7}$$

$$\frac{dv_{gz}}{dt} = - \frac{\omega_{co} v_{gx} z}{w} , \tag{8}$$

where $\omega_{co} \equiv eB_0/m_e c$. Multiplying Eq. (7) by v_{gx} and Eq. (8) by v_{gz}, adding these two equations and integrating yields

$$v_{gx}^2 + v_{gz}^2 = v_{gxo}^2 + v_{gzo}^2 \equiv v_{go}^2 \tag{9}$$

where v_{gxo} and v_{gzo} are the initial electron velocity components. Integrating Eq. (7) also yields

$$v_{gx} = v_{gxo} + \frac{\omega_{co}}{2w} (z^2 - z_o^2), \tag{10}$$

where z_o is the initial axial position of the electron when it enters the $\underline{E} \times \underline{B}$ current channel. Combining Eqs. (9) and (10) results in

$$v_{gz} = \frac{dz}{dt} = \pm \left[v_{gzo}^2 - \frac{\omega_{co} v_{gxo}}{w} (z^2 - z_o^2) - \frac{\omega_{co}^2}{4w^2} (z^2 - z_o^2)^2 \right]^{1/2} . \tag{11}$$

This equation can be solved in terms of elliptic integrals and inverted to yield z(t). Here, however, the intent is only to show that self-consistent orbits exist in the current channel and to compare the characteristic of these orbits with those seen in the simulation (see Fig. 5a).

Electrons enter the current channel at z_o with energy

$$\frac{1}{2} m_e v_o^2 \gtrsim \int_o^{z_o} \left(\frac{eE_o z}{w}\right) dz = \frac{eE_o z_o^2}{2w} , \tag{12}$$

where the inequality is used because energy acquired from the induced electric field has been neglected. In general, energy acquired from the induced fields is small compared with the energy associated with the electrostatic potential well of the current channel in the plasma. The integral can be evaluated from 0 to z_o regardless of the actual path the electron takes because the electrostatic force in conservative and the cathode is at zero potential.

If an electron enters the current channel with $v_o=v_{xo}=v_D$ (i.e., $v_{gxo}=v_{gzo}=0$) at $z_o=z_D$, then it will drift straight from the cathode end to the anode end of the current channel. From Eq. (12) one find that $z_D/w \lesssim (v_D/w\omega_{co})^{1/2} \sim 0.43$ for $v_D \sim 1.5\times10^{10}$cm/s, w ~ 1 cm and $\omega_{co} \sim 8\times10^{10}s^{-1}$ at t = 4 ns and r = 3.5 cm. Thus electrons injected near the center of $\underline{E} \times \underline{B}$ drift current channel and parallel to it will have straight line orbits as seen in Fig. 5a. Electrons injected at an angle or at some other z_o will gyrate about z_D as it travels from the cathode to the anode.

Electrons injected into the channel at z_o with $\underline{v} = v_D \hat{\underline{e}}_x + \underline{v}_{go}$ will be confined in the channel if z(t) is bounded by $w \gtrsim z(t) \gtrsim 0$. The turning points or bounds of the orbit can be found from Eq. (11) by setting $v_{gz} = 0$. For example, if $v_{gxo} = 0$, the turning points are at $z_\pm = \left(z_o^2 \pm 2wv_{gzo}/\omega_{oc}\right)^{1/2}$. Similarly, if $v_{gzo} = 0$, $z_+ = z_o$ and $z_- = \left(z_o^2 - 4wv_{gxo}/\omega_{oc}\right)^{1/2}$. An electron

entering the channel at $z_o = w$ with $v_{gzo} = 0$ and $v_{gxo} = v_o - v_D > 0$, then has turning points at $z_+ = w$ and $z_- = [w^2 - 4w(v_o - v_D)/\omega_{co}]^{1/2}$. Such an electron is confined to the channel if $z_- > 0$ or $v_o^2/v_D^2 < (1 + w\omega_{co}/4v_D)^2$. Using the same numbers as before for v_D, w and ω_{co}, this shows that electrons with energies as much as five times that associated with the drift motion ($m_e v_D^2/2 \sim 80$ keV) can be confined in the channel. Current carrying electron kinetic energies as high as ~ 400 keV are observed in the simulations at t = 4 ns.

The average gyroperiod for an electron in the current channel is $T = 2\pi w/\omega_{co}\langle z\rangle \sim 4\pi/\omega_{co}$, where $\langle z\rangle$ is the time averaged axial position. Comparing the distance an electron drifts, $v_D T$, in one gyroperiod with the axial excursion, $\Delta z = |z_+ - z_-|$, during a gyration, yields the ratio $v_D T/\Delta z \gtrsim 4\pi v_D/w\,\omega_{co} \sim 2.3$. Again the same numbers as those used following Eq. (12) were used. This result implies that the orbits will be elongated in the x direction as observed in Fig. 5a from the simulations. Thus the orbits found from Eqs. (5) and (6) quite adequately describe the electron motion in the current channel observed in the simulations.

The electron orbits shown in Fig. 5b can be used to explain the motion of the anode end of the current channel. On the generator side of the switch region electrons can enter the plasma from the anode behind the ion layer and the current channel. These electrons are initially bent away from the ion layer and current channel toward the generator by the magnetic field. However, once in the plasma, they can $\underline{E} \times \underline{B}$ drift axially toward the load and thus into the ion layer. Near the anode the $\underline{E} \times \underline{B}$ drift is predominantly axial because the E_z field must vanish at the conducting anode. The induced E_r then provides the axial drift. With electrons drifting into and neutralizing the ion space charge layer from the generator side, the electron current channel must move toward the load in order to maintain the space separation required for the proper E_z.

On the generator side of the current channel $B \sim B_0 t/\tau$ The induced E_r can be estimated using Faraday's law as $E_r \sim B_0 \ell/c\tau$, where $\ell^{-1} \sim \partial/\partial z$. The axial drift velocity then scales as $E_r c/B \sim \ell/t$. Thus the position of the anode end of the current channel,

$$z_a(t) \sim \int \ell/t \, dt \;\; \alpha \;\; \ln(t), \tag{13}$$

should have a logrithmic dependence on time. Figure 6 shows a plot of the position of the anode end of the current channel as a function of time. The behavior in time exhibited in the simulations is in very good agreement with this model. This indicates that the anode end of the current channel is controlled by electrons drifting into the ion layer from the generator side of the switch region.

The position of the cathode end of the current channel is controlled by another mechanism. As seen in Fig. 4, a dense layer of protons moves toward the load and controls the main emission site of the electrons and hence the current channel source. The motion of this channel source can be modeled using a piston or snowplow approach. This structure acts like a leaky piston because it appears to sweep up most but not all of the ions in its path and carry them along as it travels toward the load. A simple analysis of this structure in cylindrical geometry can be made. Assume that the total current in the channel of width w is supplied by electrons of uniform density n(t) traveling with the $\underline{E} \times \underline{B}$ drift provided by space charge separation. Then I(t) is given by Eq. (1) with $n(\alpha + 1)$ set equal to n(t) and r evaluated at the cathode. Ions are collected in the piston and are accelerated by the electric field in the channel such that

$$\frac{d}{dt}\left(Mn\frac{dx_p}{dt}\right) = enE, \tag{14}$$

where M is the ion mass and x_p the distance travelled by the piston. This is equivalent to a simple $\underline{J} \times \underline{B}$ acceleration of the plasma as demonstrated by noting that $enE = env_D B/c = JB/c$ where v_D is just the electron $\underline{E} \times \underline{B}$ drift velocity. Although there is charge separation in the piston (see Fig. 9b), it is assumed that the ion and electron densities averaged over the piston width are roughly equal. Thus, the density of electrons and ions in the channel is only a function of the amount of ions swept up. It is also assumed here that only a fraction, β, of the ions crossed by the piston are swept up. This is the leaky piston assumption. Then the density of current carrying electrons can be written as

$$n(t) = n_o\left(1 + \frac{\beta x_p(t)}{w}\right), \tag{15}$$

where n_o is the original plasma fill density.

Once the piston has begun to move, the electron current channel and the associated structures can be pictured as in Fig. 9b. Plasma with the original fill density, n_o, exists on both the load and generator sides of these structures. The current flows diagonally across the plasma in the higher density or piston region where there exists negative space charge. On the generator side of this current channel an equivalent positive space charge is spread over the ion layer at high density ($n_i \gtrsim n_e$) and the depletion layer ($n_o > n_i >> n_e$). The total width of the structure including the current channel, the ion layer, and the depletion layer is still $\sim 2w$ as defined in Eq. (4).

Equations (1), (14) and (15) can now be combined to obtain an equation describing the motion of the piston

$$\frac{d^2x_p}{dt^2} = \left(\frac{BI}{2\pi r_o} - \beta n_o M(dx_p/dt)^2\right)/Mwn_o(1+\beta x_p/w). \quad (16)$$

Equation (16) can be solved given the initial conditions $x_p(0)$ and $x_p'(0)$, the current, $I(t)$, the magnetic field in the channel, $B(t)$, and estimates of w and β from the simulation. Ion acceleration and collection in the piston is hampered if the electron current channel sweeps through the plasma so fast that ions cannot be picked up in the "potential well" of the $\underline{E} \times \underline{B}$ current channel. For very fast sweep speeds the piston is very leaky (i.e., $\beta \to 0$), while at slower sweep speeds more ions can be accelerated. This leakage occurs in all the cases that were simulated because the anode end of the current channel moves rapidly through the plasma. The piston is most leaky at early times when the anode end of the current channel is moving fastest. The axial acceleration of ions does not occur close to the cathode because the axial electric field vanishes there. Motion of the piston along the cathode occurs because the current channel extends diagonally across the plasma and ions are accelerated downward toward the cathode as well as axially toward the load. The position of the piston at the cathode, $z_c(t)$, is then proportional to its displacement $x_p(t)$ through

$$z_c(t) = x_p(t)/\sin\theta, \quad (17)$$

where θ is the angle made by the piston with the cathode. Results of the piston model will be shown for $z_c(t)$.

In order to test the validity of the piston model a problem is chosen where the motion of the anode and cathode ends of the channel are relatively decoupled. The best example is the C^+ problem after the anode end of the

current channel has nearly reached the load edge of the original plasma. Before this point is reached, the anode end of the current channel moves through the plasma producing little ion acceleration because of the large ion inertia (see Figs. 6 and 7). After the anode end slows down (~ 4 ns), ion acceleration can occur relatively unaffected by the motion of the anode end. Equations (16) and (17) will be used to model this situation with θ assumed constant. The initial conditions $z_c(t_o)$ and $z'_c(t_o)$ at t_o = 4 ns are taken from Fig. 7. The current, I(t), magnetic field in the channel, B(t), the channel width, w, and the "leakage" factor, β, are all taken from the simulation (Case 4, Table I).

Results are shown in Fig. 10 for $z_c(4\ ns) = 3.35$ cm, $z'_c(4\ ns) = 5.5 \times 10^8$ cm/s, r_o=2.5 cm, w=1 cm, β=0.3, $n_o = 10^{12}$ cm^{-3}, and $\theta = 30^0$. Figure 10a depicts the motion of the piston along the cathode, $z_c(t)$, and shows good agreement with the actual piston position taken from the simulation. Figures 10b and 10c plot the calculated density of the current carrying electrons (equal to the density of collected ions) and the transverse electric field in the $\underline{E} \times \underline{B}$ drift channel. These two quantities are more difficult to compare with the simulation results but there appears to be good agreement as well.

The last physical process to be described involves the current transfer to the load. Most current carrying electrons cross to the anode in the plasma, however, some electrons can leak out into the vacuum region. Electrons which exit the current channel at such an angle as to carry them into this field free region between the plasma and the load will follow ballistic orbits until striking a surface. Ions are not present in this region to provide the E_z field required for radial drifting. Some of these electrons reach the load and provide an initial load current. This load current then produces a magnetic field in the region on the load side of the

plasma which begins to magnetically insulate more of the electrons from reaching the anode as they exit the current channel. Once the anode end of the current channel reaches the load side of the original plasma region, full switch opening begins. Electrons on the generator side of the current channel continue to drift axially toward the load and neutralize the ion space charge in the electron depletion layer. Since there are no further ions to uncover on the load side, the balance between the $\underline{E}$ and $\underline{v} \times \underline{B}$ forces on the electron current channel is upset and the $\underline{v} \times \underline{B}$ force dominates. The current channel bends toward the load, and the anode end of current channel detaches from the anode. Electrons exiting the current channel are now sprayed into the vacuum region. As the load current increases, the electron current channel is pulled toward the cathode, and ions in the remaining ion layer and current channel are also swept down to the cathode. When the switch is completely open, there remains: a plasma at the anode, a gap with radial ion space charge limited current flow, and magnetically insulated axial electron current flow along the cathode surface. This final configuration is illustrated in Figs. 2e, 3e and 4e.

This section closes with a comparison of the results of the five cases from Table I. The logarithmic time dependence of the position of the anode end of the current channel as seen in Fig. 6 is expected from Eq. (13). Except for Case 2, all cases show roughly the same motion. Because of the factor of two lower density in Case 2, one would expect the depletion layer, ion layer and current channel structure to be broader. From Eq. (4) this width for Case 2 should be about twice as large as that for Case 1, as is confirmed in the simulations. If ℓ in Eq. (13) is roughly approximated by this width, then the velocity of the anode end of the current channel in Case 2 should be about twice as fast as the other cases, in agreement with what is

observed. The slightly faster motion of Cases 1 and 5 over Cases 3 and 4 is most likely a result of larger $\underline{J} \times \underline{B}$ piston motion in the body of the plasma. Piston motion is less in Case 3 because of the lower current and in Case 4 because of the higher mass.

The cathode end of the current channel behaves as would be expected from the piston model described earlier. That is, from Eq. (16), the initial acceleration of the piston is roughly proportional to the square of the current and inversely proportional to the ion mass and density. It is expected that Case 2, at half the density of Case 1, would have about twice the acceleration. Similarly, Case 3 should experience about 1/4 the acceleration because the risetime of the current has been reduced by 1/2. Case 4 should show about 1/12 the acceleration because of the higher mass of the carbon ions. The differences between Case 1 and Case 5 should be practically negligible in this context. All these predictions are qualitative confirmed in the simulations as seen in Fig. 7. It would be unrealistic to expect exact agreement between the heuristic arguments above and the actual motion of the piston's intersection with the cathode because of the strong coupling of the two ends of the current channel. However, the agreement is remarkably good as evidenced by Fig. 10.

The final comparison is the time of opening for this switch. Table II shows the time at which 90% of the total current has been diverted to the load. A comparison of these results with the results displayed in Fig. 6 shows a strong correspondence between the time of opening and the motion of the anode end of the current channel. Case 2 opens the earliest at 3.5 ns and is also the case with the fastest motion at the anode. Similarly Case 3 opens last and moves slowest at the anode. Thus it can be concluded that the motion of the anode end of the current channel determines the time of opening. If it

is assumed that ℓ in Eq. (13) is given roughly by w in Eq. (4), then qualitatively the switch will open sooner for lower n. One also finds for the cases simulated that the time of opening is basically independent of the plasma flow velocity, V_F. Evidence for this is that Cases 1 and 5 are nearly identical. The length of the switch, however, should have a strong effect on the time of opening. The longer the switch, the longer it will take for the anode end of the current channel to reach the load end of the plasma. This cannot be carried too far since the motion of the piston will eventually overtake the motion of the anode end of the current channel.

V. Conclusions

In this paper we have demonstrated some of the salient features of a simulation of a plasma switch that operates at low density ($\sim 10^{12} cm^{-3}$) and in the absence of any plasma instabilities. The simulation is done in cylindrical geometry with azimuthal symmetry and the switch operates at a plasma temperature, which for numerical reasons, is near 5 keV. Current is driven through the plasma filling the region between the anode and cathode with electron current provided by space charge limited emission of electrons at the cathode. The initial plasma has a radial flow velocity, V_F, toward the cathode and plasma is continuously injected from the anode at that flow velocity. There is no evidence of plasma instabilities or anomalous resistivity and the switch operates largely through the mechanisms of electron $\underline{E} \times \underline{B}$ drift and space charge limited emission of electrons.

Four aspects of switch behavior have been identified: 1) early current conduction and current channel formation, 2) motion of the anode end of the current channel, 3) motion of the cathode end of the current channel, and 4) switch opening. Analysis of the anode motion, cathode motion and electron

orbits in the channel has been performed, showing good agreement with simulation results.

The current channel is about 1 cm wide throughout the process. The emission site of electrons at the cathode varies in position and width during the operation of the switch. Before the development and motion of an ion "piston" through the plasma, emission is concentrated at the generator side of the cathode, with emission "enhanced" by the ion space charge exposed at the generator side of the plasma. The emission region widens slightly as the channel bends diagonally, but never becomes as broad as the original plasma region before the piston has developed. This diagonal bending occurs because the anode end of the current channel moves toward the load as electrons $\underline{E} \times \underline{B}$ drift axially into the ion layer on the generator side of the current channel.

When ions begin to be accelerated in the channel and form a piston, the piston controls the load-side end of the emission region. Emission is still locally enhanced by the ion space charge at the cathode end of the ion layer. Emission continues on the generator side of the piston, although electrons emitted there flow axially along the cathode until they reach the current channel.

Eventually, the electrons "disconnect" from the ions, i.e., the trajectories of the electrons in the current channel carry them into a region on the load side of the original plasma position where ions cannot provide the axial field required for radial $\underline{E} \times \underline{B}$ drifts. In this case the electrons can no longer cross the switch. At this point current is completely diverted to the load and any emitted electrons become magnetically insulated. The motion of the anode end of the current channel determines the time of opening which is found in the simulation to be independent of the plasma flow velocity. The motion of the anode end of the current channel, and thus time of opening, does

depend on density, moving faster for lower density. The length of the switch, however, also has a strong effect on the time of opening. The longer the switch the longer it will take for the anode end of the current channel to reach the load end of the plasma. This scaling will be limited by $\underline{J} \times \underline{B}$ effects since the piston will eventually overtake the motion of the anode end of the current channel in a very long switch.

In future work, an investigation will be made of the presence of plasma instabilities and anomalous resistivity in the switch plasma. Many instabilities cannot be simulated using the present code because of the assumption of azimuthal symmetry and the use of large mesh size and high plasma temperature. However, it may be possible to model these instabilities by introducing appropriate transport terms in the particle equations of motion. The effect of a collision term has been investigated in a steady state fluid treatment of the problem. These preliminary results show that switch behavior could be considerably altered under these conditions, giving wider current channels and more predominantly radial motion of the electrons when a sufficiently large collision frequency is used.

Acknowledgments

This work was supported in part by the U.S. Department of Energy and the Office of Naval Research. The authors wish to acknowledge L. Seftor for his assistance in setting up MASK and the members of the Plasma Technology Branch at the Naval Research Laboratory for useful discussions of the physics.

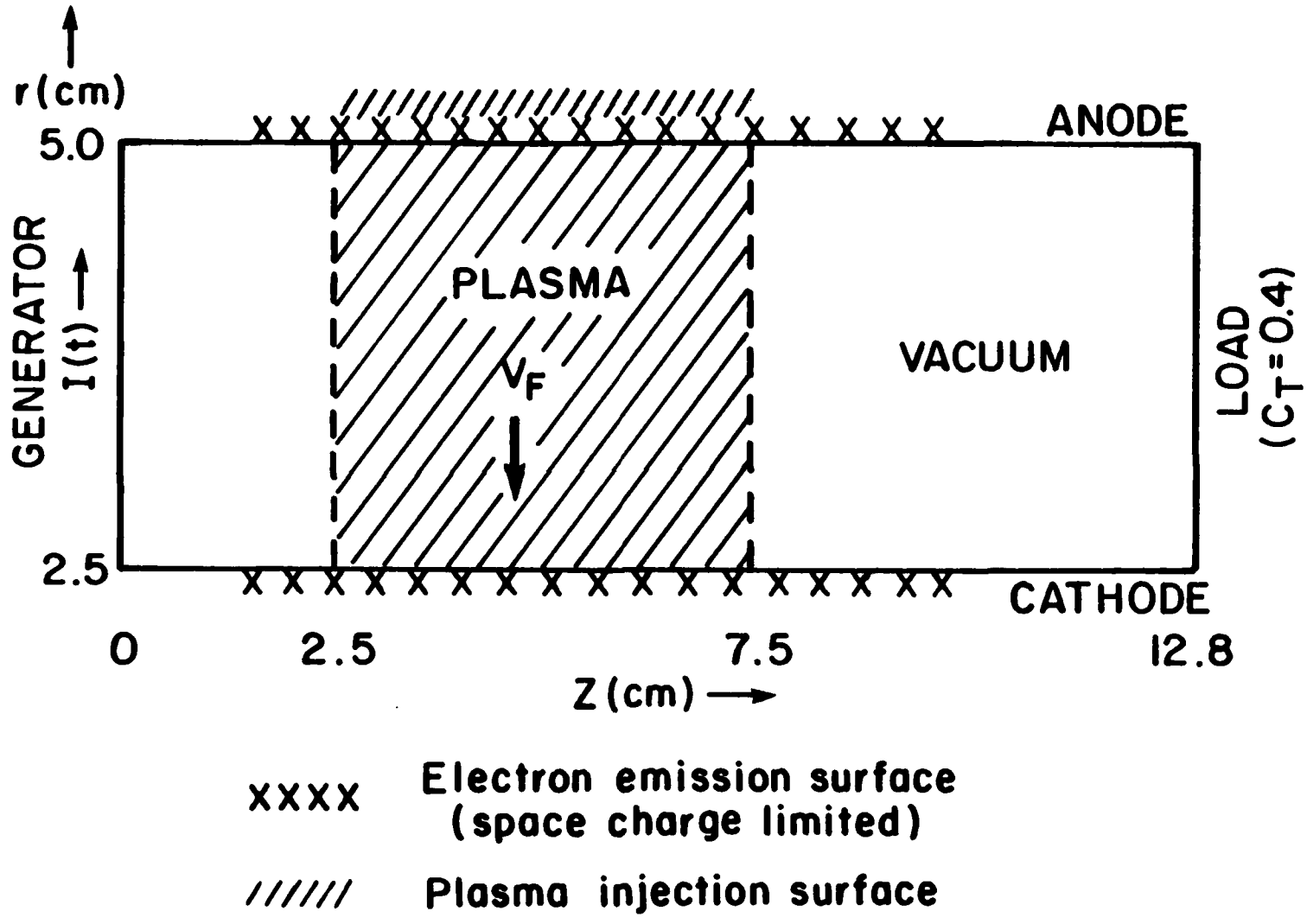

Fig. 1 — Schematic diagram of simulation region.

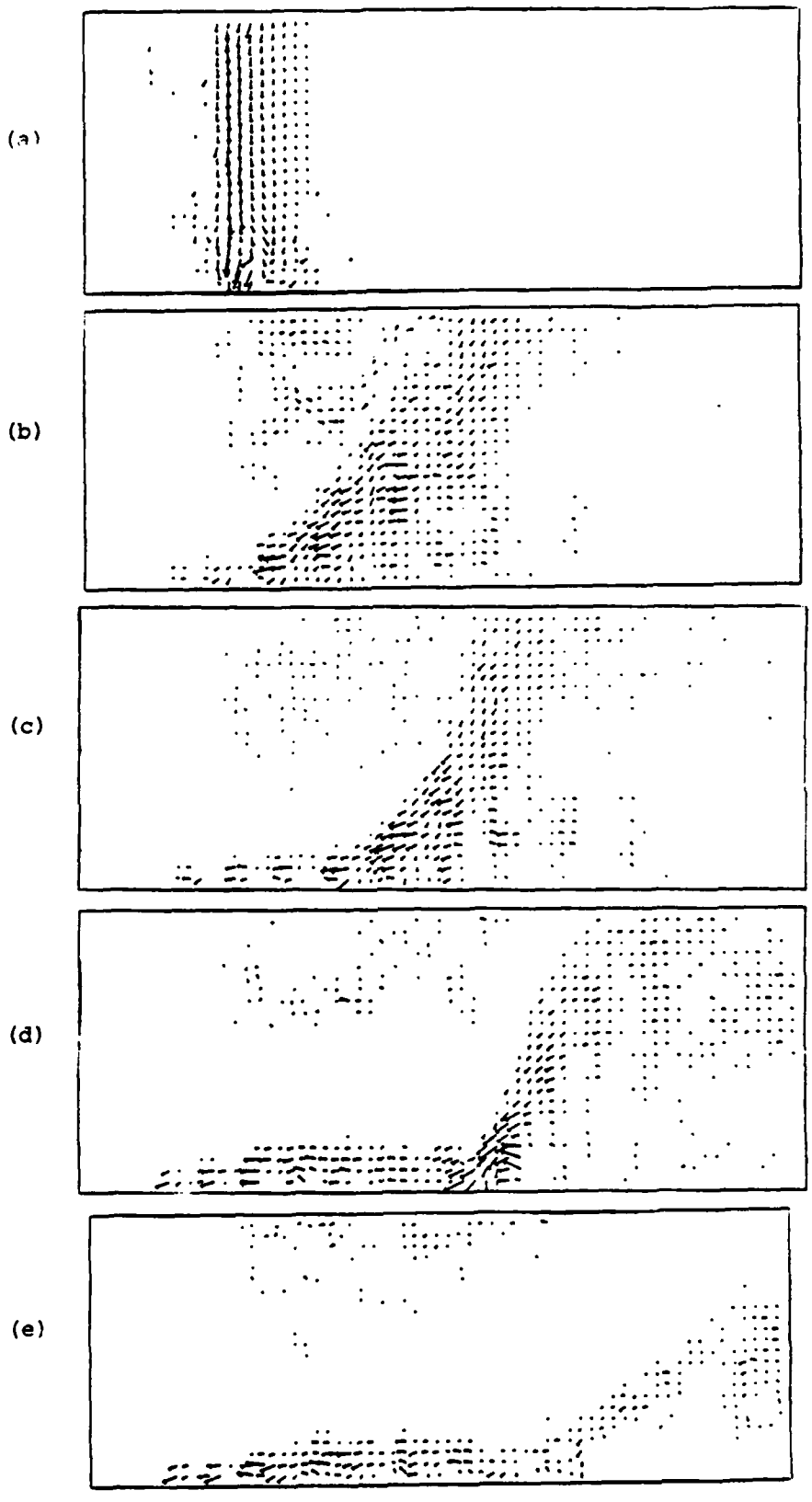

Fig. 2 — Plot of current density, $\underline{J}$, for Case 1 in Table 1 at (a) t = 0.4 ns, (b) t = 3 ns, (c) t = 4 ns, (d) t = 5 ns and (e) t = 6 ns.

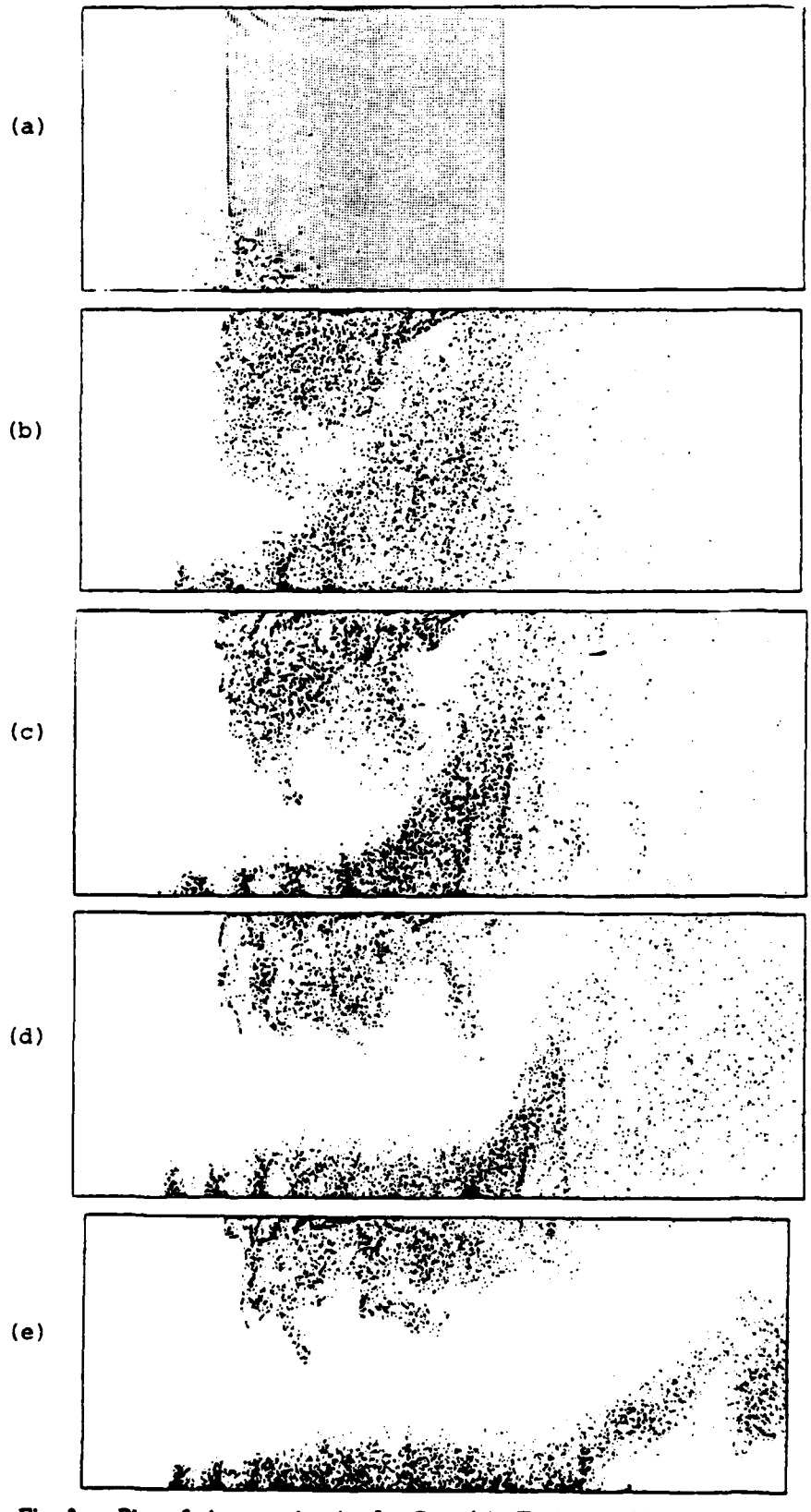

Fig. 3 — Plot of electron density for Case 1 in Table I at (a) t = 0.4 ns, (b) t = 3 ns, (c) t = 4 ns, (d) t = 5 ns and (e) t = 6 ns.

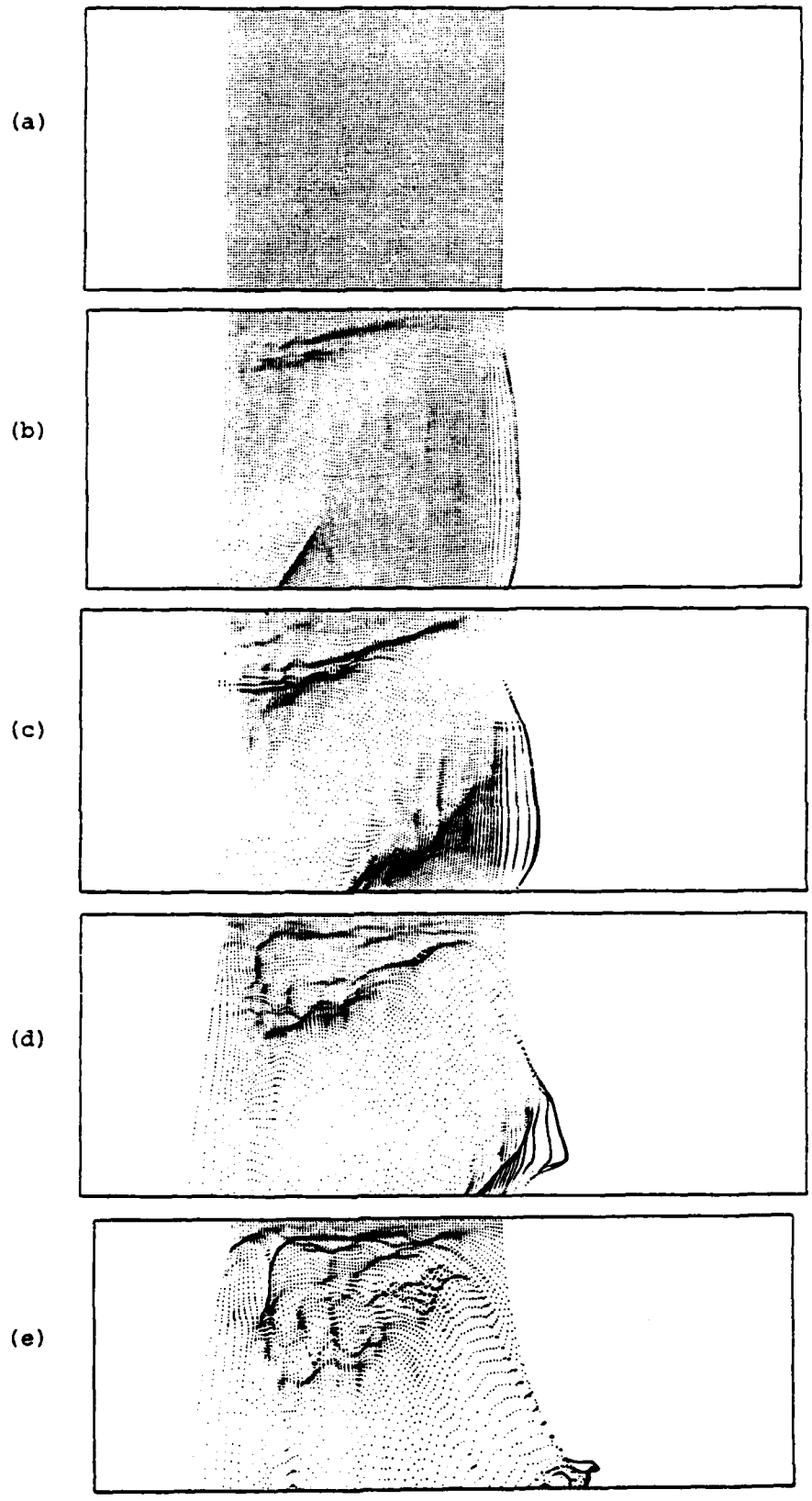

Fig. 4 — Plot of ion density for Case 1 in Table I at (a) t = 0.4 ns, (b) t = 3 ns, (c) t = 4 ns, (d) t = 5 ns and (e) t = 6 ns.

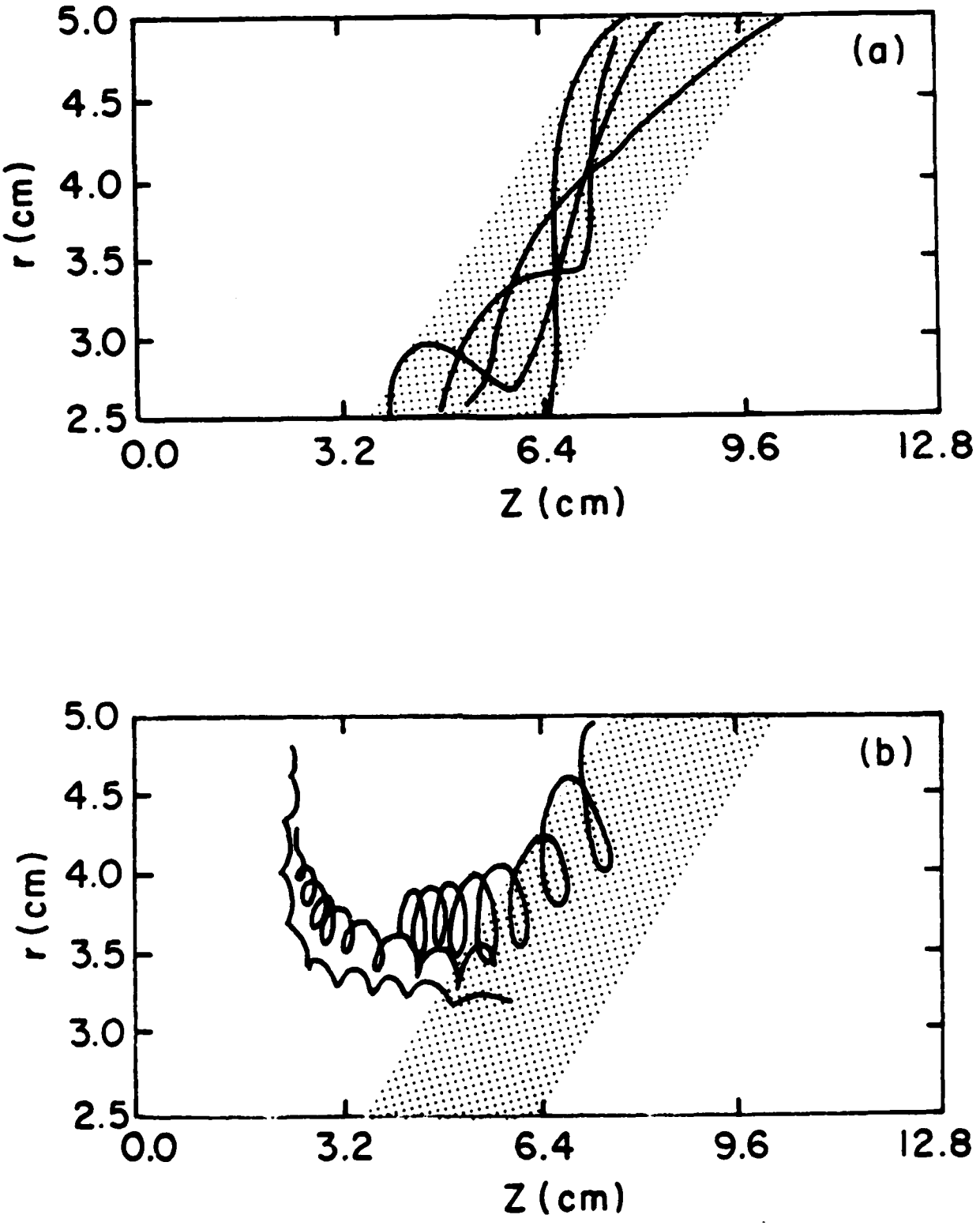

Fig. 5 — Electron trajectories for Case 1 in Table I at t ~ 4.0 ns (a) in the current channel and (b) in plasma on the generator side of the current channel. The shaded region indicates the position of the current channel.

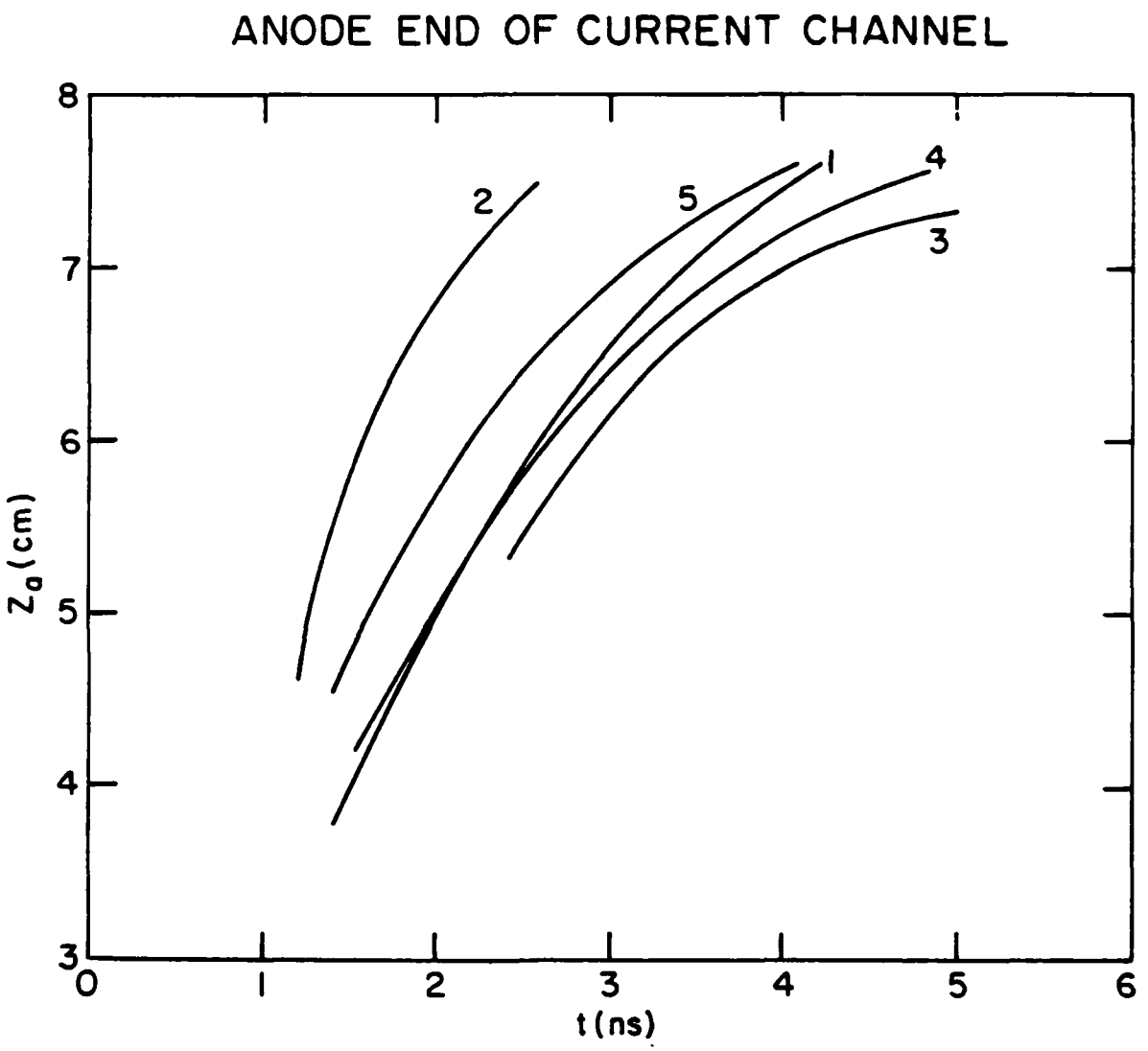

Fig. 6 — Motion of the anode end of current channel for each of the five cases in Table I.

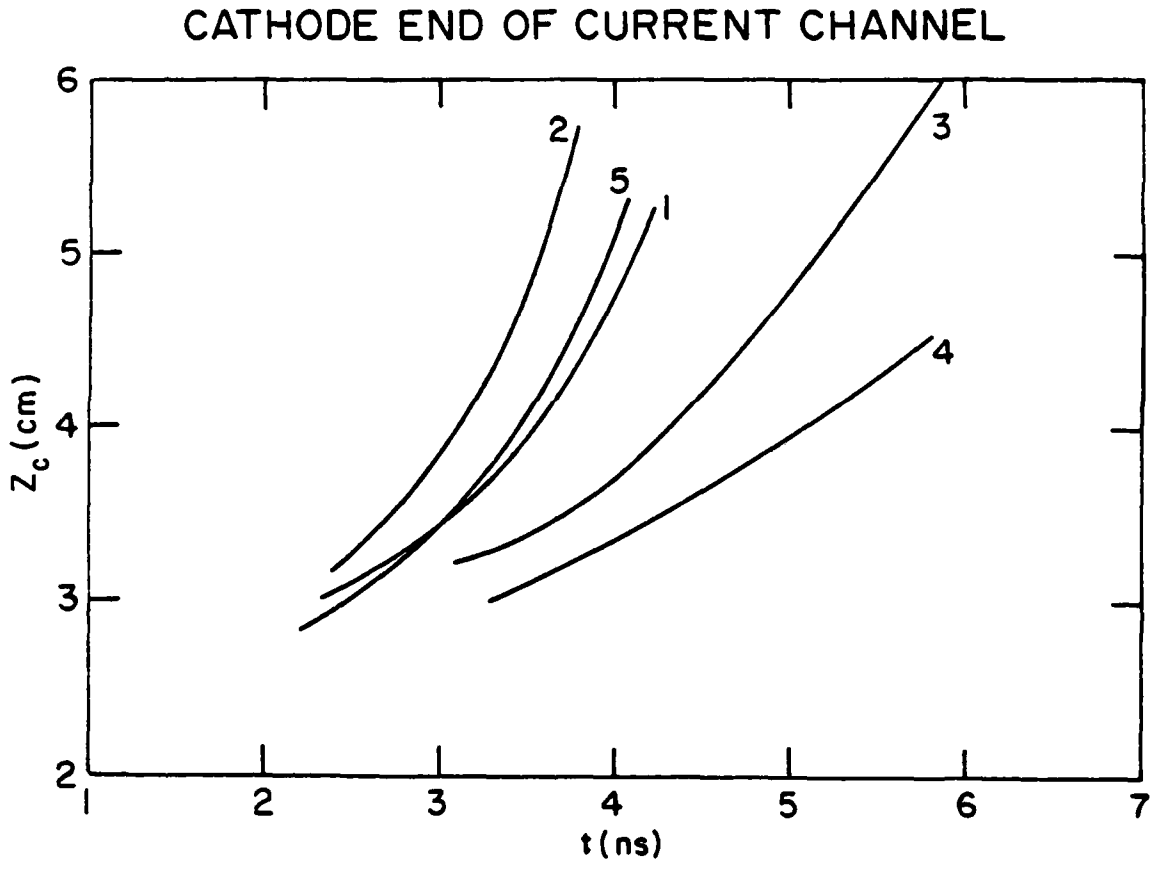

Fig. 7 — Motion of the cathode end of current channel for each of the five cases in Table I.

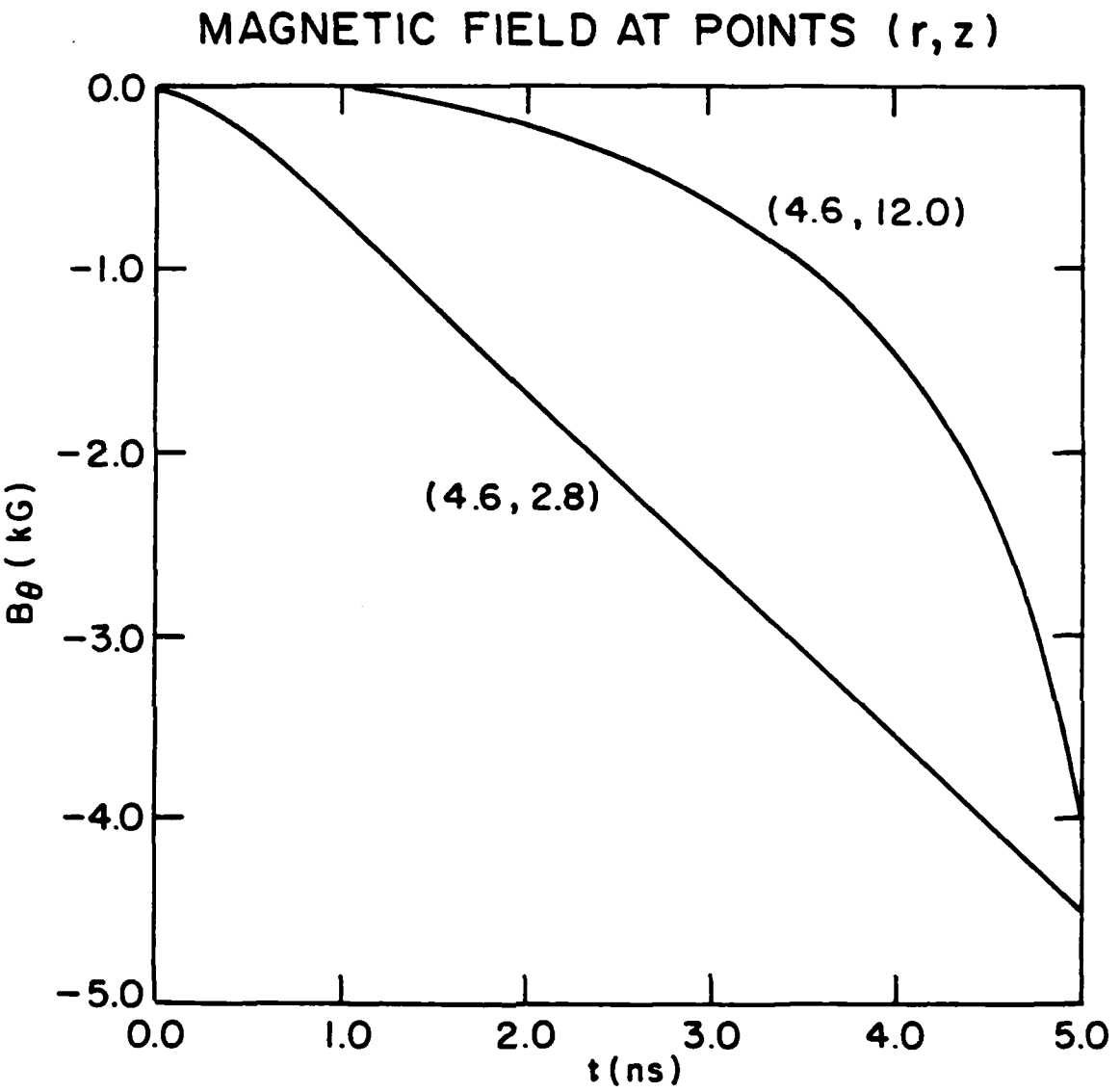

Fig. 8 — Magnetic field at (r,z) = (4.6, 2.8) and (4.6, 12.0) for Case 1 in Table I.

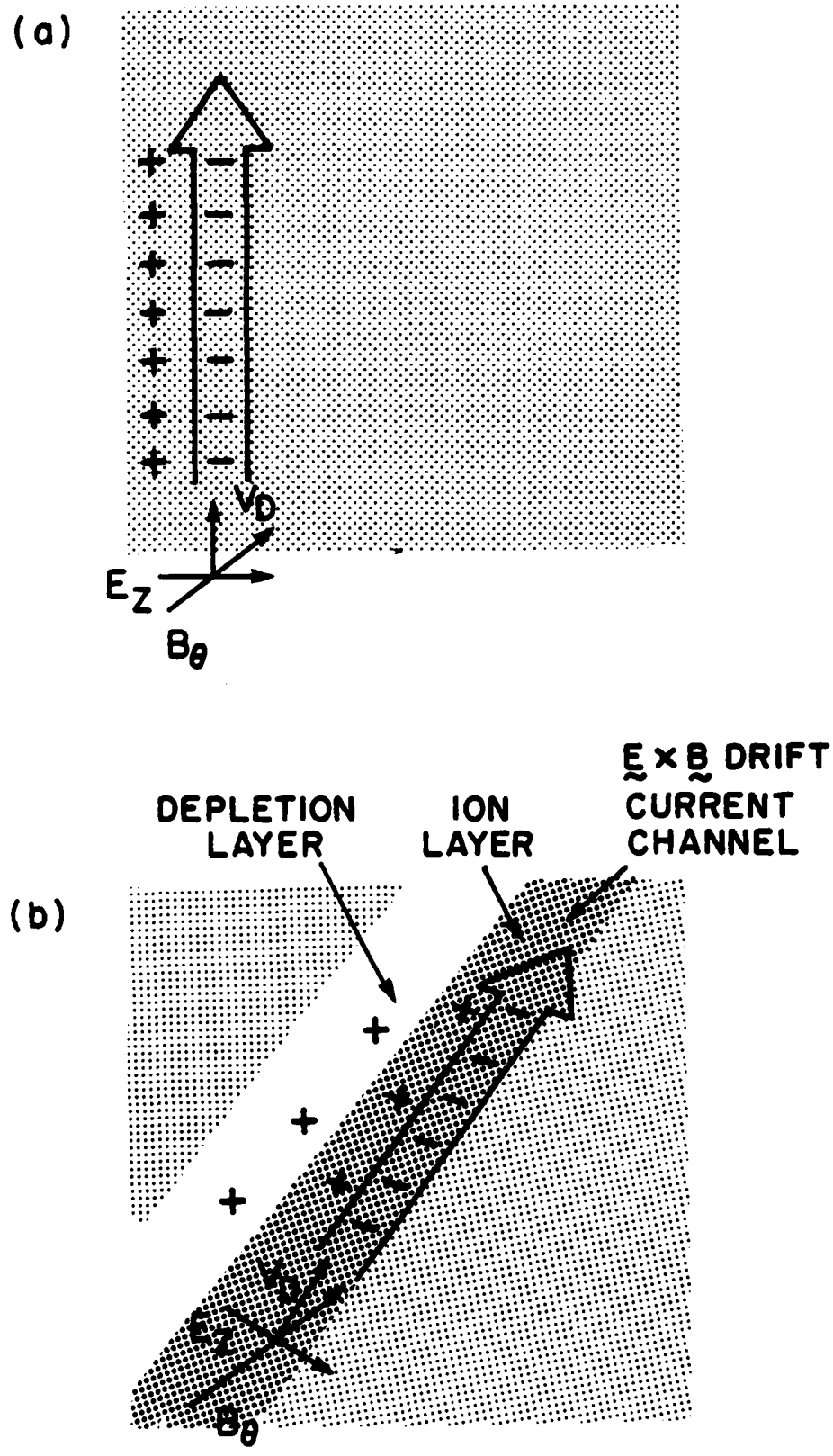

Fig. 9 — Schematic of plasma configuration (a) at early time (< 1 ns) and (b) at intermediate time (≥ 3 ns).

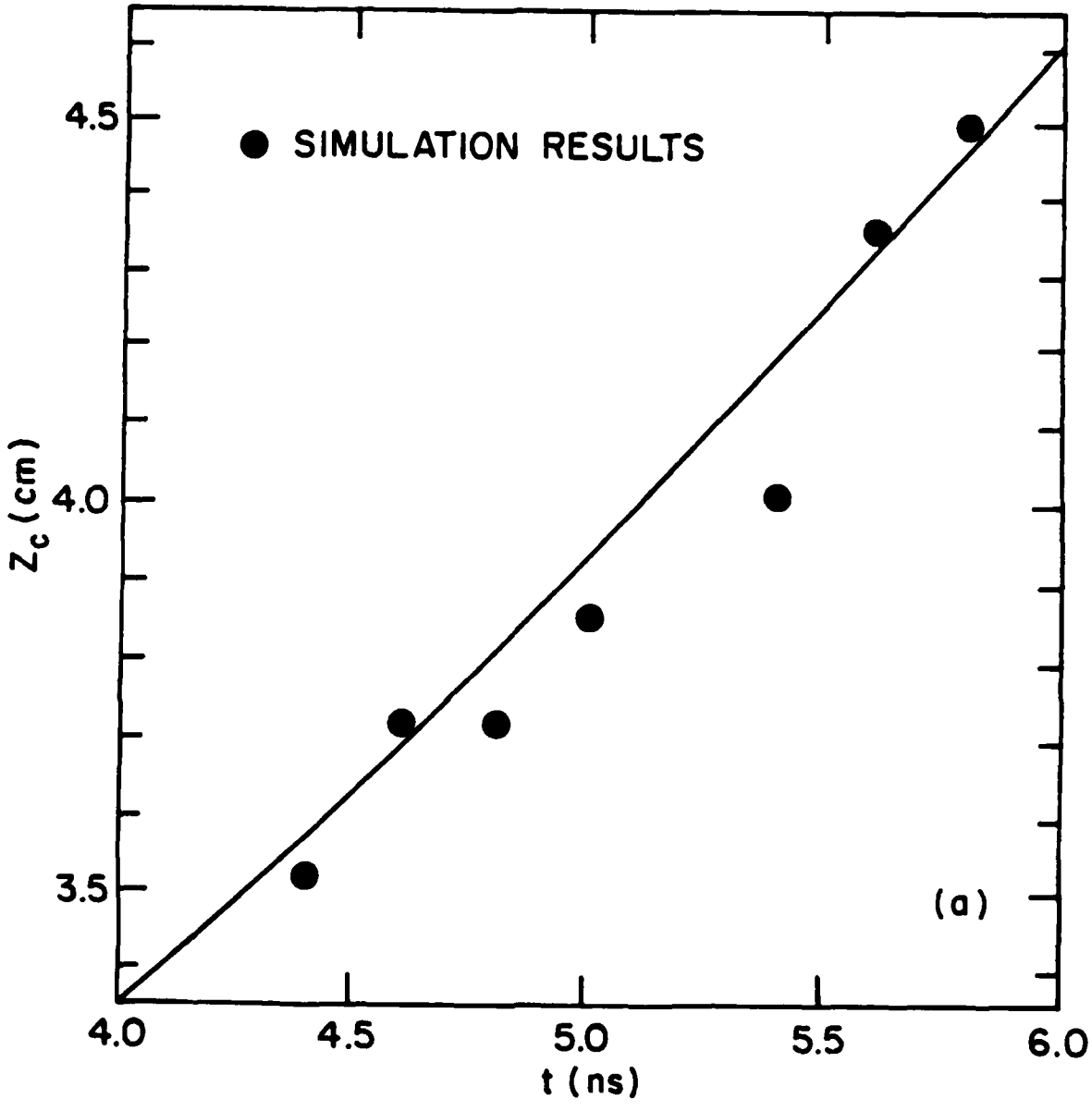

Fig. 10 — Piston model results for (a) $z_c(t)$, (b) $n(t)$ and (c) $E(t)$.

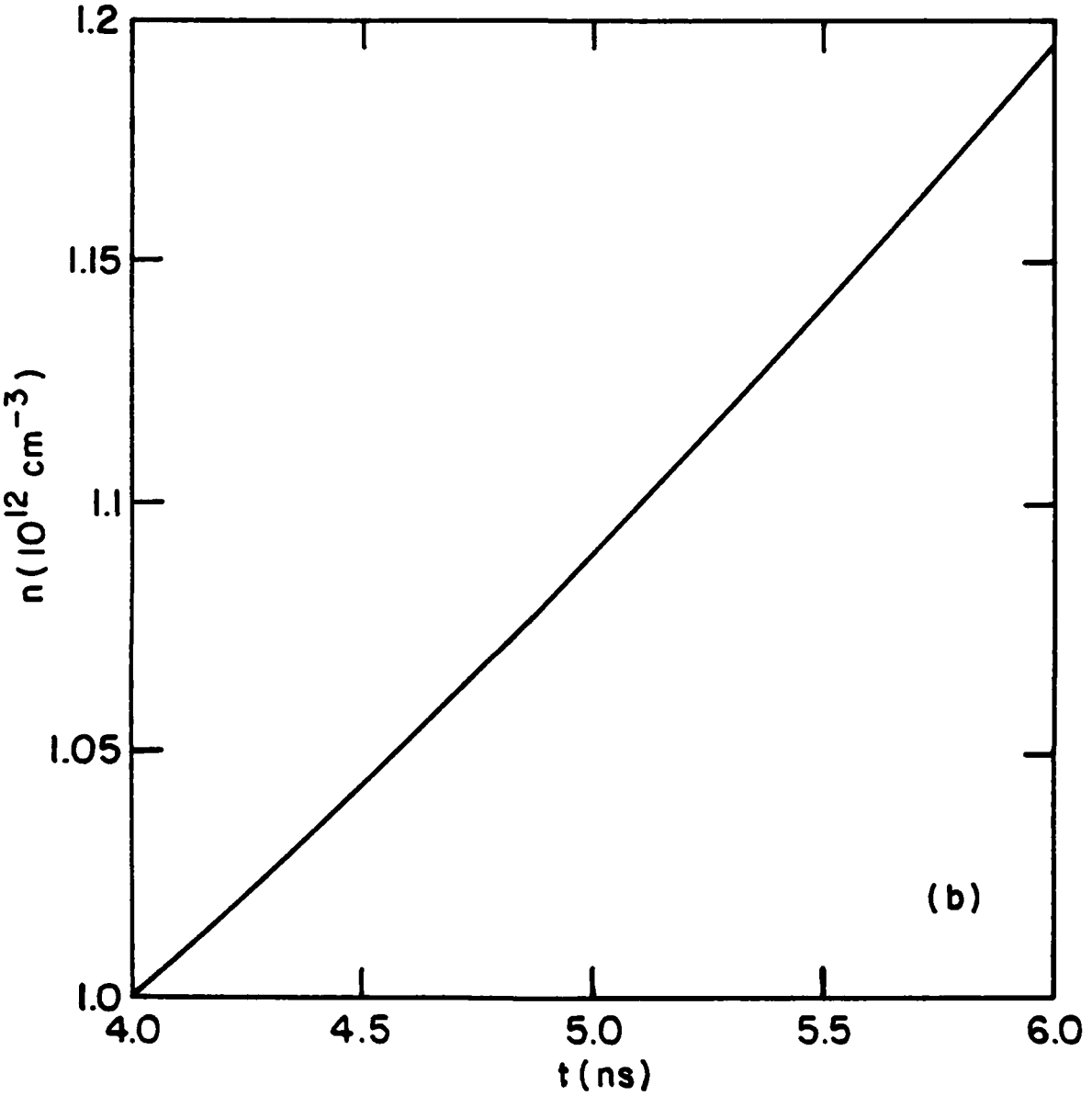

Fig. 10 (Cont'd) — Piston model results for (a) $z_c(t)$, (b) n(t) and (c) E(t).

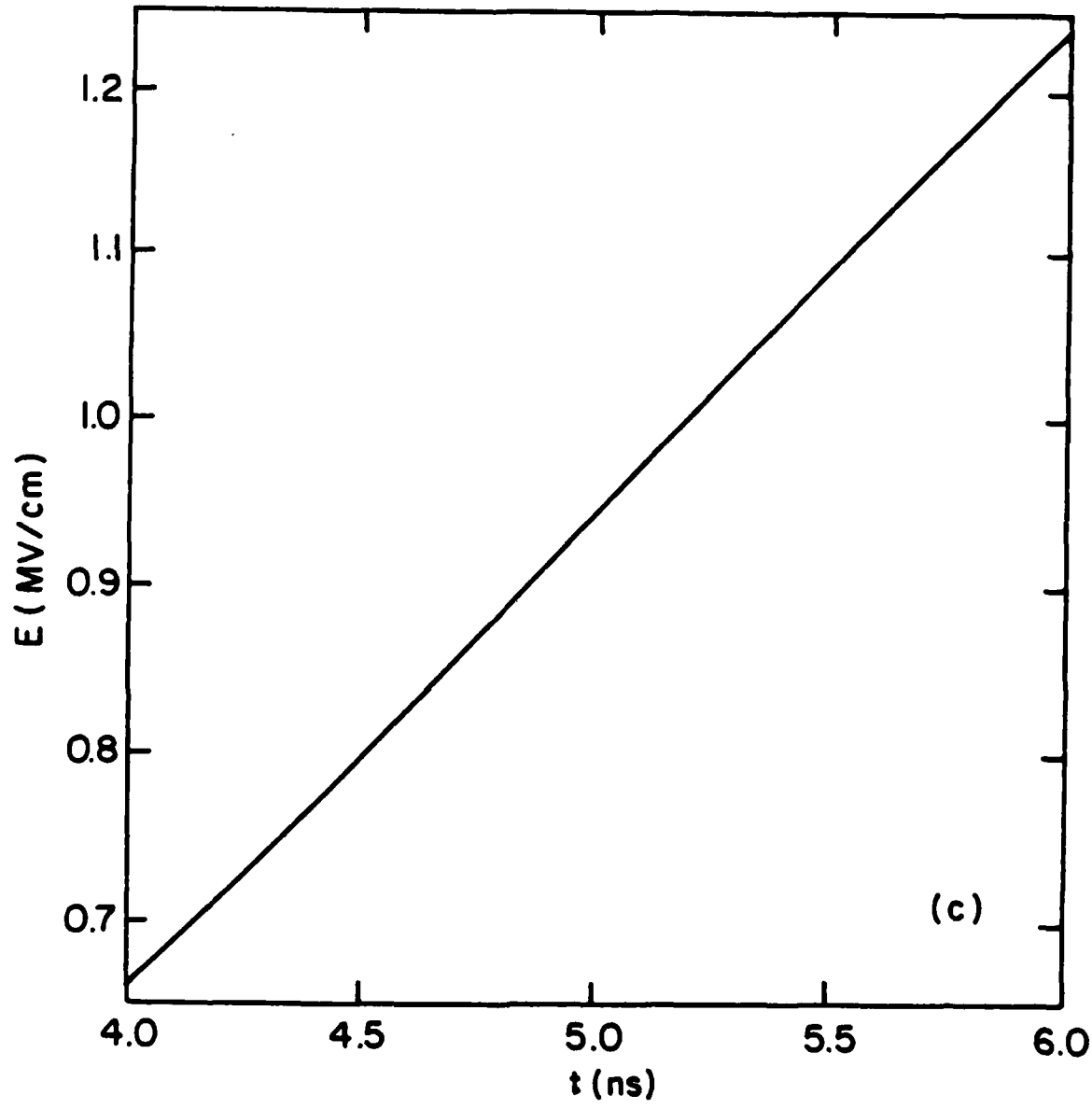

Fig. 10 (Cont'd) — Piston model results for (a) $z_c(t)$, (b) n(t) and (c) E(t).

References

1. R.A. Meger, R.J. Commisso, G. Cooperstein and Shyke A. Goldstein, Appl. Phys. Lett. 42, 943 (1983).
2. C.W. Mendel, Jr. and S.A. Goldstein, J. Appl. Phys. 48, 1004 (1977).
3. K.D. Bergeron and J.P. VanDevender, 1978 IEEE International Conference on Plasma Science (Monterey, CA, 1978), IEEE Cat. No. 78CH1357-3NPS, p. 281.
4. P.F. Ottinger, S.A. Goldstein and R.A. Meger, J. Appl. Phys. 56, 774 (1984).
5. A.T. Drobot, Bull. Am. Phys. Soc. 29, 1379 (1984); J.M. Grossmann, J.M. Neri, P.F. Ottinger and A.T. Drobot, Bull. Am. Phys. Soc. 29, 1207 (1984).
6. B.V. Weber, J.R. Boller, R.J. Commisso, J.M. Neri, W.F. Oliphant, P.F. Ottinger, T.J. Renk, S.J. Stephanakis and F.C. Young, in Proceedings of the Fifth IEEE Pulsed Power Conference (Arlington, VA, June 1985); R.J. Commisso, G. Cooperstein, R.A. Meger, J.M. Neri, P.F. Ottinger and B.V. Weber, The Plasma Erosion Opening Switch, Naval Research Laboratory Memorandum Report 5560 (May 1985). (AD A154 942)
7. P.F. Ottinger, J.M. Grossmann, A.T. Drobot, L. Seftor and R.A. Meger, 1985 IEEE International Conf. On Plasma Science (Pittsburgh, PA, June 1985), IEEE Cat. No. 85CH2199-8, p. 81.
8. E.M. Waisman, P.G. Steen, D.E. Parks and A. Wilson, Appl. Phys. Lett. 46, 1045 (1985).
9. B.V. Weber, R.J. Commisso, R.A. Meger, J.M. Neri, W.F. Oliphant and P.F. Ottinger, Appl. Phys. Lett. 45, 1043 (1984).

END

DTIC

5-86